Arabian Journal of Chemistry (2016) 9, S1131–S1137

King Saud University

Arabian Journal of Chemistry

www.ksu.edu.sa
www.sciencedirect.com

ORIGINAL ARTICLE

Magnetic properties of triethylene glycol coated $CoFe_2O_4$ and $Mn_{0.2}Co_{0.8}Fe_2O_4$ NP's synthesized by polyol method

S. Kazan [a], E.E. Tanrıverdi [b], R. Topkaya [a], Ş. Demirci [b], Ö. Akman [a], A. Baykal [b,*], B. Aktaş [a]

[a] Department of Physics, Gebze Institute of Technology, Çayırova, 41400 Kocaeli, Turkey
[b] Department of Chemistry, Fatih University, B. Cekmece, 34500 Istanbul, Turkey

Received 25 July 2011; accepted 10 December 2011
Available online 17 December 2011

KEYWORDS
Magnetic nanomaterials;
Magnetic properties;
$CoFe_2O_4$;
VSM

Abstract In this study, we reported on the structural and magnetic properties of TEG-$CoFe_2O_4$ and TEG-$Mn_{0.2}Co_{0.8}Fe_2O_4$ nanocomposites produced by the glycothermal reaction (polyol). X-ray diffraction (XRD), transmission electron microscopy (TEM) and vibration sample magnetometer (VSM) analysis have been carried out in order to understand the effect of Mn^{2+} into $CoFe_2O_4$ and it was observed that the addition of Mn^{2+} tends to reduce the crystallite size, increase the a_o (cell parameter) and increase the T_B. The presence of adsorbed polyol entities on the surface of the $CoFe_2O_4$ and $Mn_{0.2}Co_{0.8}Fe_2O_4$ NP's was also proven by TG measurements. FT-IR analysis suggested the presence of adsorbed TEG molecules on the surface of $CoFe_2O_4$ and $Mn_{0.2}Co_{0.8}Fe_2O_4$ NP's.

1. Introduction

Both $MnFe_2O_4$ and $CoFe_2O_4$ ferrites are among the widely studied ferrites because of a number of possible applications such as high frequencymagneto strictive and electromagnetic applications (Zi et al., 2009; Msomi et al., 2011). In order to change the magnetic properties, substitution of other elements such as manganese into cobalt ferrites was proposed by many researchers (Paulsen et al., 2004; Caltun et al., 2007a,b). Zhou et al. (2002) reported that thin films and fine particles of the manganese doped cobalt ferrites were found to be suitable for magneto-optical applications. Mossbauer spectroscopy investigation of $CoMn_xFe_{2-x}O_4$ was carried out by Krieble et al. (2005). The superparamagnetic properties of ferrite materials can be controlled by particle sizes and concentration of non-magnetic atoms. Efforts are being made to produce fine articles and to find dopants that can improve the properties and find new applications. Recently, interest has also shifted to Mn doped $CoFe_2O_4$ ferrites, which appear to have high stress sensitivity and large magnetomechanical effects, making these

* Corresponding author. Tel.: +90 212 8663300 2060; fax: +90 212 8663402.
E-mail address: hbaykal@fatih.edu.tr (A. Baykal).
Peer review under responsibility of King Saud University.

Production and hosting by Elsevier

http://dx.doi.org/10.1016/j.arabjc.2011.12.005
1878-5352

ferrites suitable for application as stress sensors (Msomi et al., 2011; Kambale et al., 2010; Shobana and Sankar, 2009; Shobana et al., 2009).

A number of synthetic polymers such as poly(ethylene glycol), poly(acrylamide), and poly(*N*-isopropylacrylamide), as well as naturally occurring polymers such as dextran and chitosan were used for modifying the surface properties of magnetic particles to achieve desirable surface functionalities (Takafuji et al., 2004).

Polyol process is a versatile chemical approach, which uses poly alcohols to reduce metal salts to metal particles, was successfully used to prepare a great variety of non-aggregated inorganic compounds. The polyols often serve as reaction medium with high boiling point solvent and reducing agent, as well as stabilizer to control the particle growth and prevent interparticle aggregation. The advantage of this method is the possibility to control experimental conditions and easy scale-up (Fievet et al., 1989; Feldman and Jungk, 2001; Cai and Wan, 2007; Kim et al., 2007; Chae et al., 2004; Gupta et al., 2007).

In this study, both TEG-$CoFe_2O_4$ and TEG-$Mn_{0.2}Co_{0.8}Fe_2O_4$ nanocomposites were synthesized by the glycothermal reaction (polyol) for the first time. Structural, morphological and magnetic characterization of both products was done by XRD, FT-IR, TGA, TEM and VSM methods.

2. Experimental

2.1. Instrumentation

X-ray powder diffraction (XRD) analysis was conducted on a Rigaku Smart Lab operated at 40 kV and 35 mA using Cu Kα radiation (λ = 1.54059 Å).

Fourier transform infrared (FT-IR) spectra of the samples were recorded with a Perkin Elmer BX FT-IR infrared spectrometer in the range of 4000–400 cm^{-1}.

The thermal stability was determined by thermo gravimetric analysis (TGA, Perkin Elmer Instruments model, STA 6000). TGA thermo grams were recorded for 5 mg of powder sample at a heating rate of 10 °C/min in the temperature range of 30–800 °C under nitrogen atmosphere.

VSM measurements were performed by using a Vibrating sample magnetometer (LDJ Electronics Inc., Model 9600). The magnetization measurements were carried out in an external field up to 15 kOe at room temperature.

Transmission electron microscopy (TEM) analysis was performed using a FEI Tecnai G2 Sphera microscope. A drop of diluted sample in alcohol was dripped onto a TEM grid.

2.2. Chemicals

$Co(acac)_2$, $Mn(acac)_2$, $Fe(acac)_3$, and triethylene glycol (TEG) were purchased from Merck and used as received without further purification.

2.3. Procedure

For the synthesis of TEG-$CoFe_2O_4$ nanocomposite, a stoichiometric amount of $Co(acac)_2$ and $Fe(acac)_3$ was dissolved in TEG (20 mL). And for the synthesis of TEG-$Mn_{0.2}Co_{0.8}Fe_2O_4$ nanocomposite, a stoichiometric amount of $Co(acac)_2$, $Mn(acac)_2$ and $Fe(acac)_3$ was dissolved in TEG (20 mL). Then both solutions were continuously heated to 110 °C under vigorous magnetic stirring and nitrogen atmosphere separately. After heating for 1 h, the solutions were then heated to 210 °C and kept for 2 h at this temperature. The system was then refluxed at 295 °C for 1 h. Finally the black–brown mixture (for TEG-$Mn_{0.2}Co_{0.8}Fe_2O_4$ nanocomposite) and black mixture (for TEG-$CoFe_2O_4$ nanocomposite) were cooled down to room temperature by removing the heat source. Then, ethanol was added and the solutions were centrifuged at 8000 rpm for 15 min to remove the solvent. Then obtained precipitates were washed by ethanol for three times, which could be easily dispersed in water.

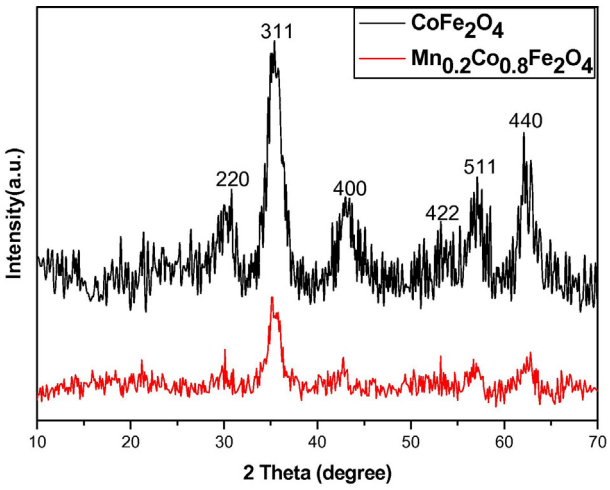

Figure 1 XRD powder patterns of as-synthesized: (a) $CoFe_2O_4$ and (b) $Mn_{0.2}Co_{0.8}Fe_2O_4$ NP's capped with TEG.

3. Results and discussion

3.1. XRD analysis

The X-ray diffraction patterns of the TEG-$CoFe_2O_4$ nanocomposite and TEG-$Mn_{0.2}Co_{0.8}Fe_2O_4$ nanocomposite (Fig. 1) show six reflection planes; (220), (311), (400), (422), (511) and (440), which indicate the presence of the spinel cubic structure

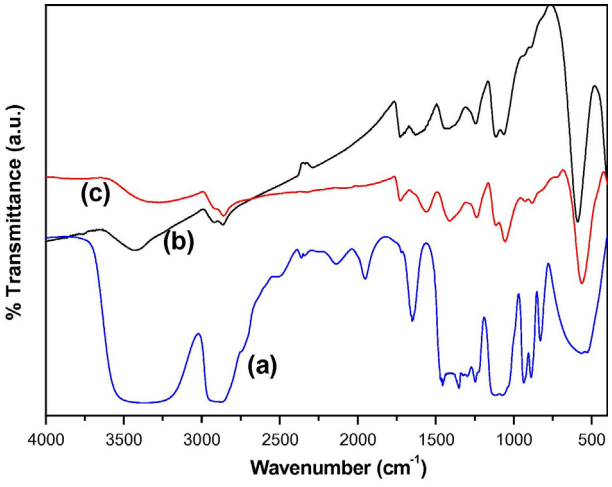

Figure 2 FT-IR spectrum of as-synthesized: (a) TEG, (b) $CoFe_2O_4$ and (c) $Mn_{0.2}Co_{0.8}Fe_2O_4$ NP's capped with TEG.

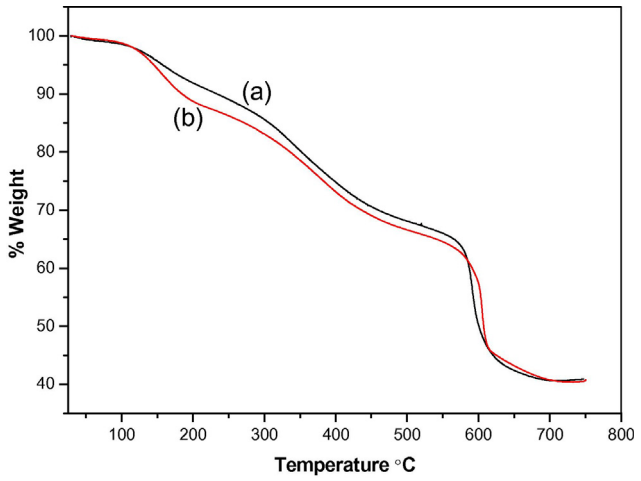

Figure 3 TGA curve of (a) $CoFe_2O_4$ and (b) $Mn_{0.2}Co_{0.8}Fe_2O_4$ NP's capped with TEG.

(El-Sayed, 2002). The lattice parameters were computed using the *d*-spacing values and the respective (*hkl*) parameters. Lattice constants of 8.381 ± 0.001 Å for $CoFe_2O_4$ (agrees with that reported in JCPDS Card No. 22-1086) were obtained compared to 8.390 ± 0.001 Å for $Mn_{0.2}Co_{0.8}Fe_2O_4$, which we may attribute to the larger size of Mn (ionic radius of 0.970 Å) substituting Co (0.885 Å). Larger Mn^{2+} replacing Co^{2+} ions therefore causing the crystal to slightly expand is in agreement with the Vegard's law (Fig. 2) (Smith and Wijn, 1959; Gao et al., 2004; Sertkol et al., 2009).

And also according to Kim et al. (2007) studyies, the absence of cubic-tetragonal (Jahn–Teller) transition in $Mn_xCo_{1-x}Fe_2O_4$ indicates a dominance of Mn^{2+} ions rather than Mn^{3+} at the octahedral sites. The octahedral Mn^{2+} (Mn^{3+}) ion in the high-spin state has an ionic radius of 0.970 Å (0.785 Å) while the octahedral Co^{2+} ion in the high-spin state has 0.885 Å. Thus, Mn^{2+} substitution for octahedral Co^{2+} can explain the increase of a_o with increasing x.

The average crystallite diameter, L, was estimated by Scherrer's equation, $L = 0.9\lambda/\beta\cos\theta_B$, from the full-width at half maximum (FWHM) of the most intense peak (311) (Chae et al., 2004; Gupta et al., 2007). The result shows that the crystallite sizes of $CoFe_2O_4$ and $Mn_{0.2}Co_{0.8}Fe_2O_4$ NP's were calculated as 5 ± 2 nm and 4.8 ± 2.1 nm respectively. The decrease in crystal size with the increase of Mn composition observed in the present work is in accordance with the earlier results of Lee et al. (1998) and Shobana et al. (2009) studies.

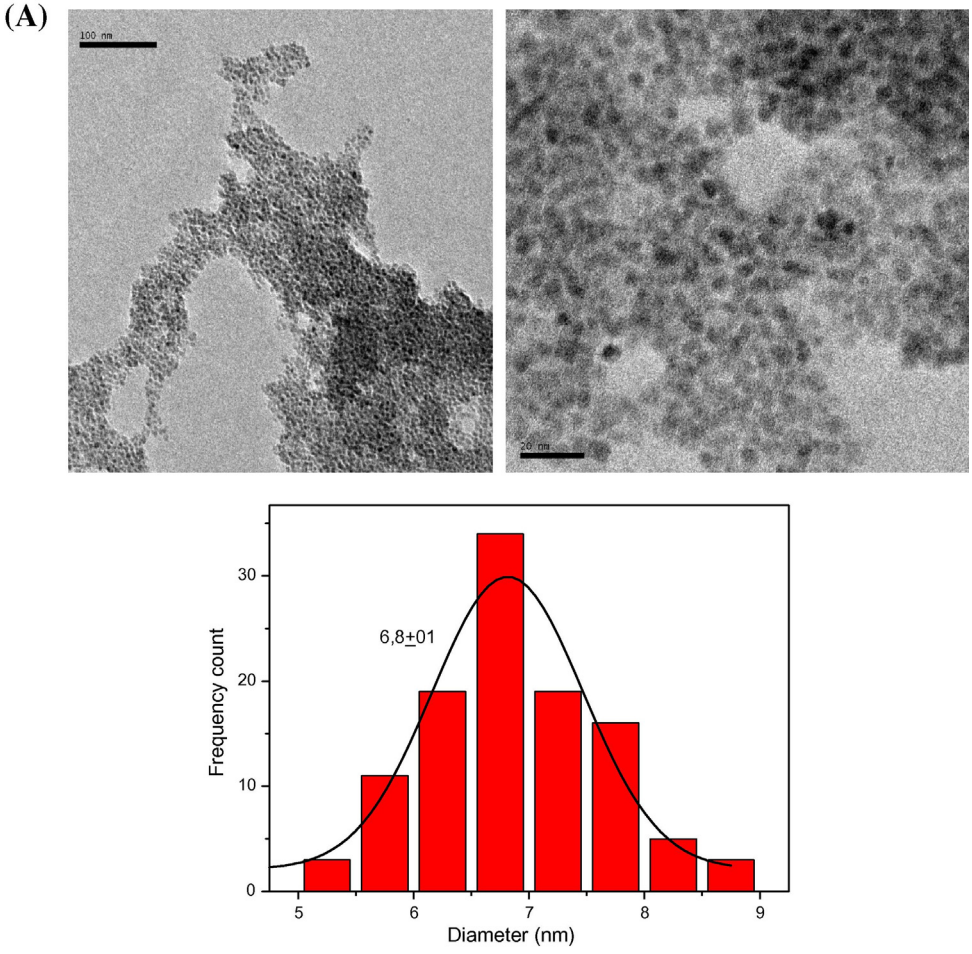

Figure 4 TEM micrographs and calculated histogram from several TEM images with log-normal fitting: (a) $CoFe_2O_4$ and (b) $Mn_{0.2}Co_{0.8}Fe_2O_4$ NP's capped with TEG.

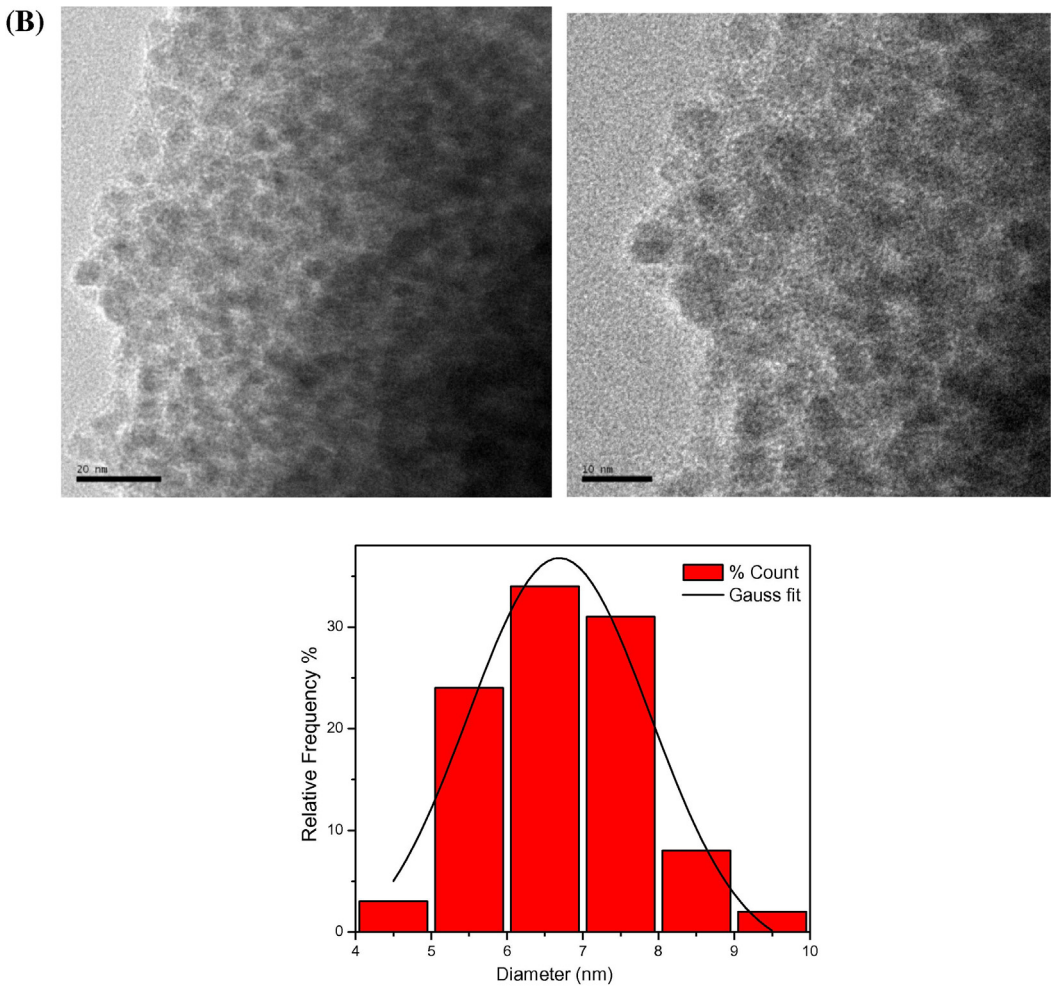

Fig. 4 (*continued*)

3.2. FT-IR analysis

The bands at 2923 and 2845 cm^{-1} were assigned to stretching of C–H groups and the bands at 1120–1060 cm^{-1} to C–O stretching surface. The broad band centered at 3430 cm^{-1} can be assigned to hydrogen bonded O–H stretching vibration arising from surface hydroxyl groups on nanoparticles and adsorbed TEG and water (Selvan et al., 2003). The absorption band at 1630 cm^{-1} on the spectra refers to the vibration of remainder H_2O in the sample (Rajh et al., 2002). FT-IR analysis suggests the presence of adsorbed TEG molecules on the surface of $CoFe_2O_4$ and $Mn_{0.2}Co_{0.8}Fe_2O_4$ NP's (Fig. 2).

3.3. TG analysis

The TG thermogram in Fig. 3 showed a minor weight-loss of 3% between 50 and 127 °C due to the loss of physically adsorbed water. The major weight-loss of 60% in the temperature range of 130–570 °C was due to the burning-off of adsorbed TEG in the sample. The weight was stabilized above 570 °C indicating all decomposition processes being completed. The presence of adsorbed polyol entities on the surface of the $CoFe_2O_4$ and $Mn_{0.2}Co_{0.8}Fe_2O_4$ NP's was also proven by TG measurements (Altincekic et al., 2010).

3.4. TEM analysis

Powder morphology was also investigated by transmission electron microscopy (TEM). A typical TEM picture was shown in Fig. 4 for $CoFe_2O_4$ and $Mn_{0.2}Co_{0.8}Fe_2O_4$ NP's. The nano- particles for both compounds consist of spherical particles. For $CoFe_2O_4$ and $Mn_{0.2}Co_{0.8}Fe_2O_4$ NP's, the average particle size, as observed by TEM measurements, were found to be 6.8 ± 0.1 and 6.9 ± 0.2 nm, respectively. These values were in agreement with estimates from the XRD data.

3.5. VSM measurements

We have investigated the magnetic properties of $CoFe_2O_4$ and Mn doped $CoFe_2O_4$ nanoparticles by measuring the magnetization in both zero-field-cooled (ZFC) and field-cooled (FC) modes under 50 Oe magnetic fields as shown in Fig. 5. As shown in Fig. 5 the variation of the magnetization in FC and ZFC modes indicated the superparamagnetic behavior in which the FC and ZFC curves coincide at high temperature then start to separate from each other with decreasing temperature. In the ZFC curve, the magnetization started to increase slowly with increasing temperature until it reaches a maximum value where the thermal energy becomes comparable with the

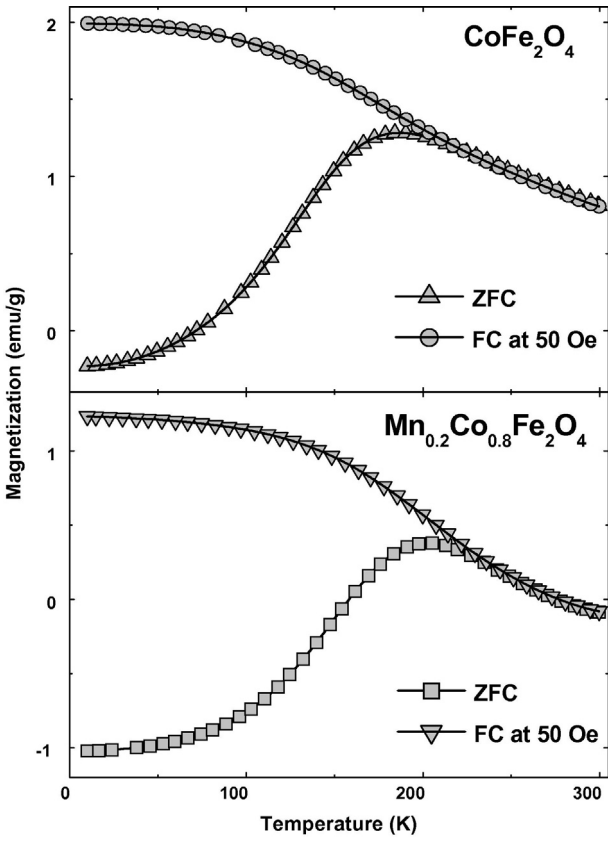

Figure 5 Magnetization (M) versus temperature (T) measured in both FC and ZFC mode for $CoFe_2O_4$ and $Mn_{0.2}Co_{0.8}Fe_2O_4$ NP's capped with TEG.

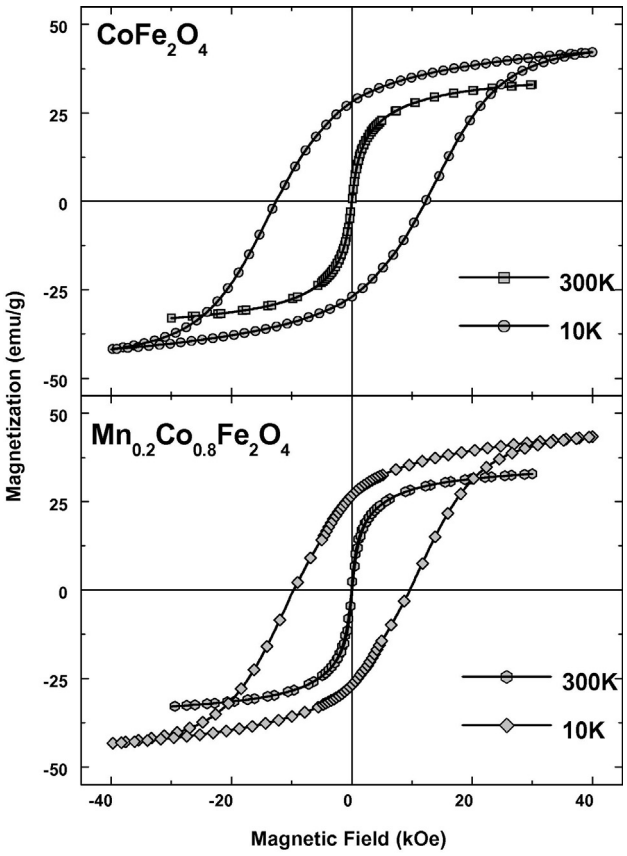

Figure 6 Magnetic hysteresis curves, $M(H)$, obtained at different temperatures above and below T_B for $CoFe_2O_4$ and $Mn_{0.2}Co_{0.8}Fe_2O_4$ NP's are capped with TEG.

anisotropy energy and then started to decrease suddenly. This temperature is known as blocking temperature and we measured 187 K for $CoFe_2O_4$ and 201 K for $Mn_{0.2}Co_{0.8}Fe_2O_4$ NP's. The variation of the blocking temperature by adding Mn ions was attributed to the changing of effective magnetic anisotropies of $CoFe_2O_4$ NP's (Melikhov et al., 2006; Kambale et al., 2010).

The magnetic hysteresis loops of the doped and un-doped samples are shown in Fig. 6 at two different temperatures (below and above the T_B) in a magnetic file up to ± 40 kOe. The saturation magnetization (M_s) of pure $CoFe_2O_4$ and Mn doped $CoFe_2O_4$ is about 33 and 32 emu/g at 300 K respectively. Further increase in doping of Mn decreases the strength of exchange interactions, and therefore the saturation magnetization decreased as reported by earlier studies (Lee et al., 1998; Caltun et al., 2007a,b; Palamaru et al., 2008). The magnetic hysteresis loop above the blocking temperature behaves as a paramagnetic.

The magnetization of ferrites which has a spinal structure depends on the distribution of magnetic moments in tetrahedral and octahedral sites (Qi and Wu, 2008). The $CoFe_2O_4$ known as inverse spinal structure and in which one-eighth of the tetrahedral sites is occupied by Fe^{+3} ions and one-half of octahedral sites are occupied by divalent Co^{+2} and Fe^{+3} ions (Sawatzky et al., 1968). The manganese substituted cobalt ferrite exhibited different magnetic behavior at low temperature as seen in Fig. 7. The magnetization of the manganese substituted cobalt ferrite is almost the same with un-doped

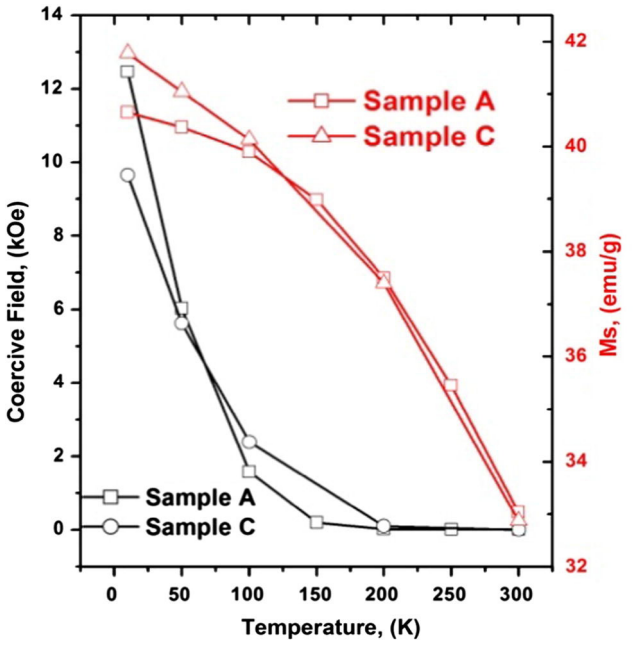

Figure 7 Variation of coercive field and saturation magnetization with temperature for $CoFe_2O_4$ (Sample A) and $Mn_{0.2}Co_{0.8}Fe_2O_4$ (Sample B) NP's capped with TEG.

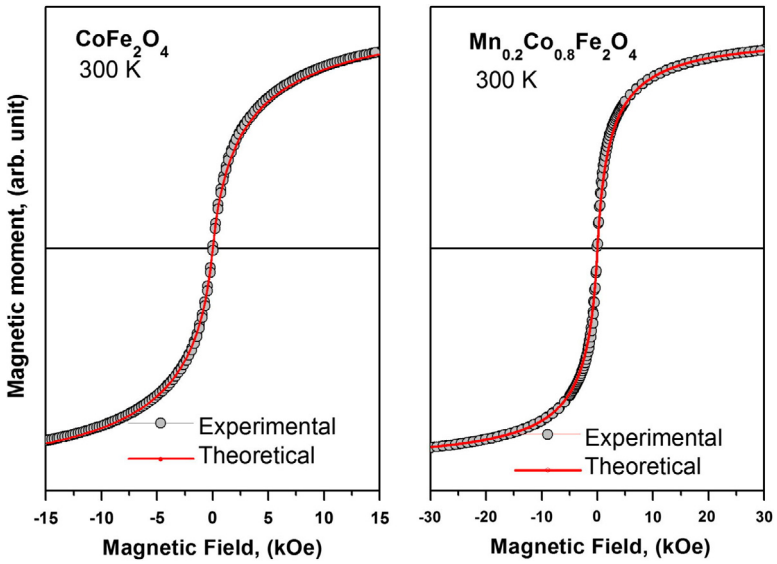

Figure 8 M vs. H curves at room temperature, 300 K, and their size-weighted Langevien fits for $CoFe_2O_4$ and $Mn_{0.2}Co_{0.8}Fe_2O_4$ NPs.

Table 1 Statistical median size (d_m), geometric standard deviation (σ_m) and average diameter (D_m) of $CoFe_2O_4$ and $Mn_{0.2}Co_{0.8}Fe_2O_4$ NP's obtained from VSM measurements.

Sample	Lattice constant (Å)	Density (g/cc)	Saturation magnetization M_s (emu/g)	d_m	σ_m	D_m
$CoFe_2O_4$	8.37	5.29	35	6.6	0.97	6.63
$Mn_{0.2}Co_{0.8}Fe_2O_4$	8.39	5.23	35.5	6.0	1.3	6.65

cobalt ferrite nanoparticles. The distribution of cations (such as Mn) in the spinel structure may directly influence the magnetic properties of materials. If the Mn concentration in $Mn_xCo_{1-x}Fe_2O_4$ NP's is higher than $x \geqslant 0.2$ value the, the magnetic properties have not been affected with the increasing Mn concentration (Sawatzky et al., 1968; Msomi et al., 2011; Melikhov et al., 2006). The coercive field of Mn doped sample decreased as a contrast to saturation magnetization at low temperature. There are a lots of attributions in the literature about how the substation sites of doped Mn ions in spinel ferrite structure depend on the magnetic measurements (Sawatzky et al., 1968; Msomi et al., 2011; Melikhov et al., 2006; Kim et al., 2006; Kundu and Mishra, 2008; Abdallah et al., 2010). The charge compensation and the occupied tetragonal/octahedral sites by doped ions may be investigated with different experimental techniques.

The room temperature magnetic hysteresis curves of $CoFe_2O_4$ and $Mn_{0.2}Co_{0.8}Fe_2O_4$ are well fitted with the size distributed Langevien function (Abdallah et al., 2010) as seen in Fig. 8.

$$M(D,H) = \sum M_i V_i f(d_i) L(x_i) \tag{1}$$

where M_i and V_i, magnetization and volume of ith particle, respectively and $f(d_i)$ is the log-normal function of $f(d_i) = 1/(\sqrt{2\pi}\ln\sigma_m)\exp(-(\ln d - \ln d_m)^2/2\ln\sigma_m^2)$ (Abdallah et al., 2010; Yakushiji et al., 2000; Kavas et al., 2009) depend on the statistical median d_m and geometric standard deviation of σ_m, and $L(x_i) = \coth(x_i) - 1/x_i$ with $x_i = M_i H V_i/kT$. The average diameter from magnetic measurement, which is denoted as D_m in Table 1, is expressed as the average diameter and is obtained by:

$$D_m = \frac{\sum d_i f(d_i)}{n} \tag{2}$$

The magnetic sizes are found to be 6.66 nm for $CoFe_2O_4$ and 7.38 mm $Mn_{0.2}Co_{0.8}Fe_2O_4$ NPs and all $d_{m,}$ σ_m *and* D_m values are tabulated in Table 1.

4. Conclusion

TEG-$CoFe_2O_4$ and TEG-$Mn_{0.2}Co_{0.8}Fe_2O_4$ nanocomposites have been synthesized by the glycothermal reaction (polyol) process. XRD diffraction and transmission electron microscopy analyses of both TEG-$CoFe_2O_4$, and TEG-$Mn_{0.2}Co_{0.8}Fe_2O_4$ nanocomposites indicated the presence of the spinel cubic structure and confirming the single crystalline nature of the nanoparticles in the products. Both TEG-$CoFe_2O_4$ and TEG-$Mn_{0.2}Co_{0.8}Fe_2O_4$ nanocomposites exhibited super paramagnetic behavior with a blocking temperature of 187 K and 201 K respectively. The VSM results showed an increment of the blocking temperature and a decrement of the coercive field with the doping of Mn ions into $CoFe_2O_4$ NP's related to effective magneto crystalline anisotropy of nanoparticles.

Acknowledgements

The authors are thankful to the Fatih University, Research Project Foundation (Contract No.: P50020902-2) and the

TUBITAK (Contract No.: 110T487) for financial support of this study.

References

Abdallah, H.M.I., Moyo, T., Msomi, J.Z., 2010. J. Phys. Conf. Ser. 217, 012141.

Altincekic, T.G., Boz, I., Baykal, A., Kazan, S., Topkaya, R., Toprak, M.S., 2010. J. Alloys Compd. 493, 493.

Cai, W., Wan, J., 2007. J. Colloid Interface Sci. 305, 366.

Caltun, O., Chiriac, H., Lupu, N., Dumitru, I., Rao, P.B., 2007a. J. Optoelectron. Adv. Mater. 9, 1158.

Caltun, O., Rao, G.S.N., Rao, K.H., Rao, B.P., Dumitru, I., Kim, C.O., Kim, C.G., 2007b. J. Magn. Magn. Mater. 316, 618.

Chae, K.P., Lee, J., Kweon, H.S., Lee, Y.B., 2004. J. Magn. Magn. Mater. 283, 103.

El-Sayed, A.M., 2002. Ceram. Int. 28, 363.

Feldman, C., Jungk, G.O., 2001. Angew. Chem. Int. Ed. 40, 359.

Fievet, F., Lagier, J.P., Blin, B., Beaudoin, B., Figlarz, M., 1989. Solid State Ionics 32–33, 198.

Gao, J., Cui, Y., Yang, Z., 2004. Mater. Sci. Eng. B 110, 111.

Gupta, N., Verna, A., Kashyap, S.C., Dube, D.C., 2007. J. Magn. Magn. Mater. 308, 137.

Kambale, R.C., Shailkh, P.A., Harare, N.S., Bilur, V.A., Kolekar, Y.D., Bhosale, C.H., Rajpure, K.Y., 2010. J. Alloys Compd. 490, 568.

Kavas, H., Baykal, A., Toprak, M.S., Köseoğlu, Y., Sertkol, M., Aktaş, B., 2009. J. Alloys Compd. 479, 49.

Kim, K.J., Kim, H.K., Park, Y.R., Park, J.Y., 2006. J. Korean Phys. Soc. 49, 1024.

Kim, K.J., Kim, H.K., Park, Y.R., Choi, S., Kim, S.E., Lee, H.J., Park, J.Y., Kim, S.J., 2007. J. Magn. Magn. Mater. 310, e618.

Krieble, K., Shaeffer, T., Paulsen, J.A., Ring, A.P., Lo, C.C.H., Synder, J.E., 2005. J. Appl. Phys. 97, 10F101.

Kundu, T.K., Mishra, S., 2008. Bull. Mater. Sci. 31, 507.

Lee, D.H., Kim, H.S., Yo, C.H., Ahu, K., Kim, K.H., 1998. Mater. Chem. Phys. 57, 169.

Melikhov, J.E.S., Jiles, D.C., Ring, A.P., Paulsen, J.A., Lo, C.C.H., Dennis, K.W., 2006. J. Appl. Phys. 99, 08R102.

Msomi, J.Z., Abdallah, H.M.I., Moyo, T., Lančok, A., 2011. J. Magn. Magn. Mater. 323, 471.

Palamaru, M.N., Iordan, A.R., Aruxandei, C.D., Gorodea, I.A., Perianu, E.A., Dumitru, I., Feder, M., Caltun, O.F., 2008. J. Optoelectron. Adv. Mater. 10 (7), 1853.

Paulsen, J.A., Ring, A.P., Lo, C.C.H., Synder, J.E., Jiles, D.C., 2004. Presentation W27-5. American Physician Physical Society, March Meeting Montreal, Quebec, Canada.

Qi, X., Wu, D., 2008. J. Magn. Magn. Mater. 320, 666.

Rajh, T., Chen, L.X., Lukas, K., Liu, T., Thurnauer, M.C., Tiede, D.M., 2002. J. Phys. Chem. B 106, 10543.

Sawatzky, G.A., Woude, F., Morrish, A.H., 1968. J. Appl. Phys. 39, 1204.

Selvan, R.K., Augustin, C.O., Berchmans, L.J., Saraswathi, R., 2003. Mater. Res. Bull. 38, 41.

Sertkol, M., Koseoglu, Y., Baykal, A., Kavas, H., Bozkurt, A., Toprak, M.S., 2009. J. Alloys Compd. 486, 325.

Shobana, M.K., Sankar, S., 2009. J. Magn. Magn. Mater. 321, 599.

Shobana, M.K., Sankar, S., Rajendran, V., 2009. J. Mater. Chem. Phys. 113, 10.

Smith, J., Wijn, H.P.J., 1959. Ferrites, vol. 44. Philips Techno Library, Eindhowen, Netherlands.

Takafuji, M., Ide, S., Ihara, H., Xu, Z., 2004. Chem. Mater. 16, 1977.

Yakushiji, K., Mitani, S., Takanashi, K., Ha, J.G., Fujimori, H., 2000. J. Magn. Magn. Mater. 212, 75.

Zhou, B., Zhang, Y.W., Liao, C.S., Cheng, F.X., Yan, C.H., 2002. J. Magn. Magn. Mater. 247, 70.

Zi, Z., Sun, Y., Zhu, X., Yang, Z., Dai, J., Song, W., 2009. J. Magn. Magn. Mater. 321, 1251.